

Highly efficient antifouling property based on self-generating hydrogel layer of polyacrylamide coatings

Gang Wu, Chang-Cheng Li, Xiao-Hui Jiang, Liang-Min Yu

Key Laboratory of Marine Chemistry Theory and Technology, Ministry of Education, Ocean University of China, Qingdao 266100, People's Republic of China

Correspondence to: L.-M. Yu (E-mail: yuyan@ouc.edu.cn)

ABSTRACT: Pursuit of robust antifouling coatings is a persistent objective for marine materials. We present here the experimental realization of a series of polyacrylamide-based resins with a self-generating hydrogel layer, arising from the polymerization of acrylamide (AM), butyl acrylate, methacrylic acid, and AM derivatives. The mechanical strength and thermal stability are markedly enhanced due to the change of the structure of modified resins. The preliminary results indicate that resultant resins with crosslinking structure show satisfactory abrasion resistance and swelling properties. The results of antifouling panel testing in shallow submergence for three months reveal that the addition of AM derivatives leads to generation of a thin soft and dynamic layer of hydrogel, which enhances antifouling properties. The formation of hydrogel and self-generating property make it promising in various antifouling applications.

© 2016 Wiley Periodicals, Inc. *J. Appl. Polym. Sci.* **2016**, *133*, 44111.

KEYWORDS: coatings; crosslinking; radical polymerization; resins; surfaces and interfaces

Received 5 April 2016; accepted 27 June 2016

DOI: 10.1002/app.44111

INTRODUCTION

Marine biofouling usually refers to the rapid growth of marine organics and some harmful and wasteful accumulation on the surface of materials immersed in seawater. The vigorous growth of marine organisms can increase surface roughness and weight, resulting in reduced ship speed, high frictional resistance, and increased fuel consumption.^{1,2} In addition, biofouling can cause the invasion of alien aquatic species, leading to ecological damage. Biofouling generally undergoes three stages: (i) adsorption of some organics on the surface as an initial accumulation; (ii) formation of a thin film of biological species on the surface along with colonies of other living microorganisms, such as bacteria, protozoa, and single-cell diatoms; and (iii) surface settlement and growth of macrofoulers, such as tubeworms, barnacles, and macro-algae.^{3,4} In this complex process, physicochemical factors of a submerged surface, such as surface tension and energy,⁵ surface chemistry,⁶ and topography,⁷ can affect biofouling. Moreover, planktonic bacteria will approach and attach to the surface through various bacteria-surface interactions (e.g., van der Waals forces, hydrogen bonding, ionic interactions, and hydrophobic interactions).⁸

Two strategies are commonly used to inhibit bacterial colonization on surfaces, namely, repelling of bacteria by antifouling coating and killing of bacterial cells with a nonleaching bactericidal layer.⁹ Antifouling coatings mainly rely on the formation

of a hydrated barrier to prevent bacterial attachment.^{10–13} Thus, creating advanced antifouling coatings is crucial to solve these limitations. Self-polishing antifouling coatings, such as a self-polishing resin, antifouling agents, and other additives, are preferred in modern antifouling techniques. Bio-inspired self-cleaning materials have recently provided new insights into the design of a highly efficient and nontoxic antifouling coating,¹⁴ from the antifouling and self-cleaning capability of fish. This principle is mainly ascribed to the fact that the low-surface-energy feature of the self-cleaning surfaces may reduce the intermolecular forces between the foulants and the surfaces. Thus, the foulants are removed by low hydrodynamic shear forces exhibiting antifouling property.^{15,16}

Soft and wet materials containing significant amounts of water are promising environment-friendly antifouling materials that can reduce contact area and surface energy.^{17–19} Hydrogels are chemically crosslinked polymers or polymer composites with 3D frameworks, which can swell in aqueous solution under osmotic pressure.²⁰ Designing an interpenetrating network structure is a useful method to enhance the mechanical strength of hydrogel materials.²¹ Recently, Xie et al.²² successfully developed a class of crosslinked hydrogels for marine antifouling applications. However, swollen hydrogels are easily damaged by an external force because of their poor mechanical properties and insufficiently strong adhesion to a surface. Hence, hydrogels

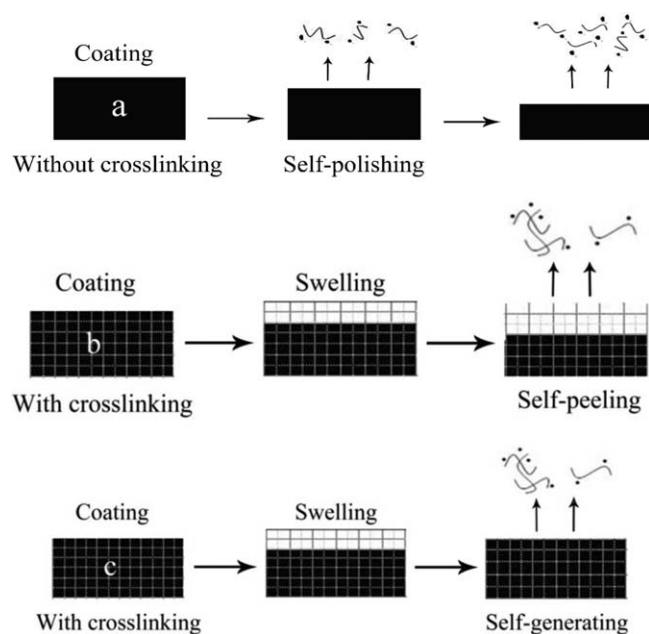


Figure 1. Schematic of self-polishing processes of (a) uncrosslinked and (b) self-peeling hydrogel coatings as well as (c) crosslinked self-generating hydrogel coatings in seawater.

are difficult to apply on a ship surface or other similar surfaces, thereby restricting their field tests and practical applications, as schematically shown in Figure 1.²² As such, a technique that can enhance the adhesion, mechanical strength, and environmental stability of hydrogels for antifouling coatings should be urgently developed.

Many studies have investigated functional hydrogels and their properties. However, the antifouling property, particularly that from the molecular structure, needs further improvement. This study introduces a simple method to design polyacrylamide-based hydrogels to evaluate their antifouling property. In this work, a set of resins, that is, C-1, C-2, C-3, and C-4, consisting of different ratios of acrylamide (AM) derivatives are synthesized by micelle copolymerization in a mixed solvent. Each resin is subsequently mixed with a polyfunctional axiridine crosslinker (TTMAP) in a stoichiometric ratio before coating on a surface. The resulting coatings are denoted as CT-1, CT-2, CT-3, and CT-4. Moreover, the mixed liquor of xylene and *n*-butanol (4:1 by mass) is used as the reaction solvent instead of water to examine the antifouling properties of the aforementioned compounds. Our main consideration in coming to replace solvent was ascribed to decrease the resins dissolved in seawater in the evaluation of the antifouling property and improve the antifouling property of the resins. The antifouling properties of the

prepared resins are evaluated by static degradation, dynamic abrasion, swelling, and panel tests in seawater. The antifouling properties are inferred to rise from the self-generation characteristic of the hydrogel, while the interior crosslinked resin provides adhesion force and mechanical property.

EXPERIMENTAL

Materials

Butyl acrylate (BA), methacrylic acid (MAA), AM, N-methylol acrylamide (N-MA), 2-acrylamide-2-methylpropanesulfonic acid (AMPS), azobisisobutyronitrile (AIBN), polyfunctional axiridine crosslinker (TTMAP), xylene, and *n*-butanol were purchased from sinopharm Reagent Company. Indoor use of sea water came from the Yellow Sea. Moreover, *N,N'*-[(2-hydroxy-4,5-dimethylbenzene-1,3-diyl)-dimethanediyl]bisprop-2-enamide (HDDE) was a kind of capsaicin derivative, which was synthesized in our own laboratory,²³ and other reagents were used as received without further purification.

Synthesis of Copolymer Resins

The copolymers were synthesized by free radical polymerization. In details, the solvent including a mixture of xylene and *n*-butanol (4:1 by mass) was placed in a three-necked flask equipped with an agitator, a dropping funnel and a reflux condenser; 30 vol % monomer mixture added to the 3-necked flask was heated to 80 °C under nitrogen atmosphere for half an hour, and then 70 vol % residual monomer mixture was added in batches and simultaneously initiator was added dropwise into the flask at a constant speed over a period of 2 h. After elevating temperature to 90 °C, an initiator (AIBN) was added into abovementioned reagent after half an hour. The polymerization continued for another 4 h at 90 °C (total initiator: 1 wt % of total monomer content). The synthetic products were stored for subsequent processing and the chemical compositions of different resins are summarized in Table I.

Coating Preparation

The copolymer resins without adding crosslinker that were prepared (C-1, C-2, C-3, and C-4) in solution can be directly applied on a surface. Coatings CT-1, CT-2, CT-3, and CT-4 were prepared by mixing the solutions of copolymers C-1, C-2, C-3, and C-4 with TTMAP in a stoichiometric ratio at the room temperature for about 20 min. Figure 2(a) shows the resin synthesis and the coating formation. Figure 2(b) shows schematic representation of the molecular C-1, C-2, C-3, and C-4 structure units in the most stable configuration. At first, the viscosity and color of the resins were not changed after adding a crosslinker. However, the viscosity of the resins quickly increased and solidified to form the gel an hour later, while the color was still not changed.

Table I. Compositions of Different Resins Synthesized by Copolymerization Reactions

Copolymers	BA/(mol %)	MAA/(mol %)	AM/(mol %)	N-MA/(mol %)	AMPS/(mol %)	HDDE/(mol %)
C-1	72	18	10	—	—	—
C-2	72	18	9	—	—	1
C-3	72	18	7	3	—	—
C-4	72	18	8	—	2	—

MEASUREMENT OF PROPERTIES

Adhesion and Stress Measurement

Three coatings were prepared using tin plate [Figure 3(c)] in accordance with the Chinese National Standard GB/T1727-1992.²⁴ The drying adhesion of the coatings was determined by a QFZ-film adhesion tester at constant temperature and humidity conditions when the coating was fully cured. The amount of adhesive force was determined by the integrity degree of the scratch. Each sample was uniformly brushed thrice to control the thickness at 300 μm .

The tensile strength was tested using a steel column with a diameter of 20 mm, in accordance with the Chinese National Standard GB/T5210-2006.²⁵ At first, we polished steel columns with sandpapers (No. 240) and cleaned, then brushed the coating to the bottom of steel columns and dried for 15 days at 37 °C to test the tensile strength, which controlled thickness at 80 \pm 20 μm . The tensile strength of the coating was tested using the AGS-J universal tensile machine.

Dynamic Abrasion Measurement

Each coating was applied on the ABS panel (350 \times 100 \times 3 mm³), and the thickness was controlled at around 300 μm [Figure 3(a)]. The panels were polished with sandpapers (No. 80) to facilitate the attachment of resin. Figure 3(d) shows the schematic illustration of the rotating experiment installed for simulated seawater. The abrasion rates of resins were determined after the coatings were dried using the laboratory rotating device for simulated seawater on the coating of the dynamic stroking water. The initial weight of the coatings after drying was measured. Subsequently, the coating panels were fixed on the rotating device for stroking water. The seawater exhibited the following characteristics: pH, 8.2; salinity, 29‰; speed, 75 rpm; and one stroke cycle, 7 days. After the end of an experimental period, the coating panels were retrieved and washed with deionized water, dried, and weighed. Weight loss was defined as the difference in the coating weight before and after stroking water. The abrasion rate (*A*) was calculated as follows:

$$A\% = \frac{W_0 - W_t}{W_0} \times 100\% \quad (1)$$

where W_t is the weight of the abrasion coating and W_0 is the weight of the coating at former cycle.

Static Degradation Measurement

Each coating was applied on the ABS panel (100 \times 80 \times 2 mm³), and the thickness was controlled at around 300 μm [Figure 3(b)]. The panels were immersed in static sea water for 10 days (pH 8.2 and salinity 29‰). The panels were then dried and weighed. After the end of an experimental period, the coating panels were retrieved and washed with deionized water, dried, and weighed. The immersion experiment can reflect the degradation ability of the coatings in seawater, that is, the self-peeling effect. The degradation rate (*D*) was calculated as follows:

$$D\% = \frac{m_0 - m_t}{m_0} \times 100\% \quad (2)$$

where m_t is the weight of the degradation coating and m_0 is the weight of immersed coating at former cycle.

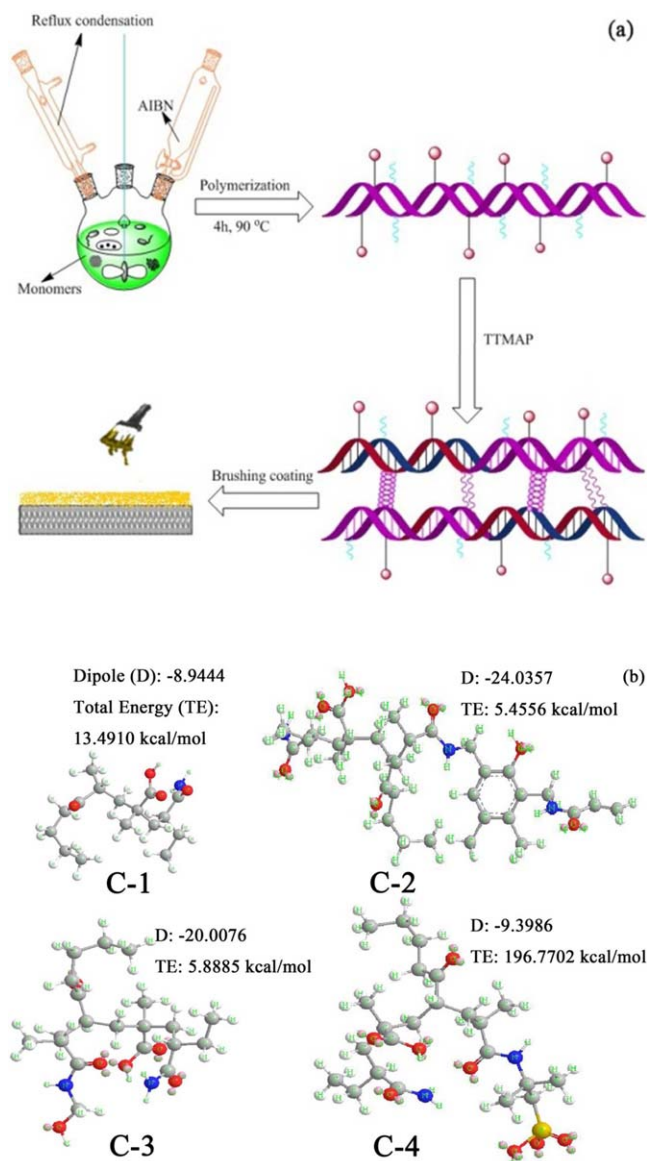


Figure 2. (a): Schematic illustration of resin synthesis and coating preparation; (b) Schematic representation of the molecular C-1, C-2, C-3, and C-4 structure units. [Color figure can be viewed in the online issue, which is available at wileyonlinelibrary.com.]

Swelling Property Measurement

Each coating was applied on the ABS panel (100 \times 80 \times 2 mm³), and the thickness was controlled at \sim 300 μm . The weight of the initial coating was determined after drying, and the samples were then immersed in the seawater tank. The test panels were weighed at specific intervals with excess moisture being removed using clean tissues. The swelling property is the difference between the weights of the coatings that showed the water adsorption property. The swelling rate (*S*) was calculated as follows:

$$S\% = \frac{M_t - M_0}{M_0} \times 100\% \quad (3)$$

where M_t is the weight of the immersed coating and M_0 is the weight of the immersed coating at former cycle.

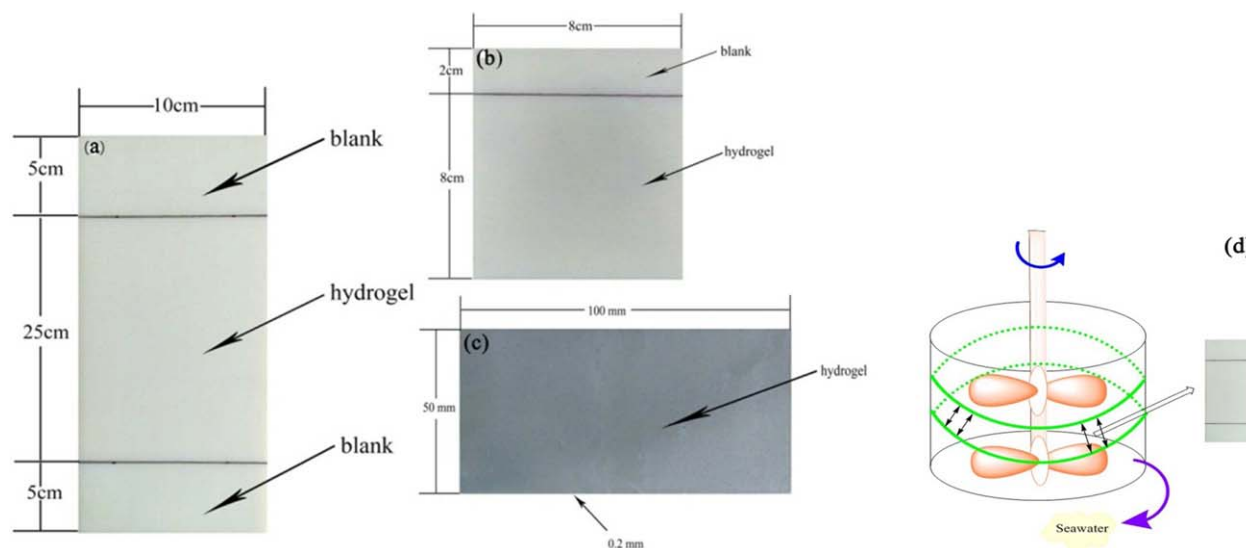


Figure 3. Schematic illustration of the ABS panels (a, b) and tin plate (c) with resins; (d) Schematic illustration of rotating experiment for simulated seawater. [Color figure can be viewed in the online issue, which is available at wileyonlinelibrary.com.]

Antifouling Property Test

The antifouling tests were performed in accordance with the GB/T5370-85²⁶ procedure. Each PVC panel ($900 \times 300 \times 3 \text{ mm}^3$) was rubbed with sandpaper. The coating was brushed to form a film of $\sim 600 \mu\text{m}$ in thickness. Afterward, the coatings were dried at 25°C for 15 days. Two similar panels were prepared for each coating and attached to a frame; these panels were submerged to a depth of 1.5 m measured from the top of the sample to the water surface from a stationary experimental buoy that was positioned in a sheltered bay with weak water currents at Qingdao, China on July 2, 2014. The testing panels were retrieved from the sea, gently washed with seawater, and photographed. The biofouling extent was then quantified by the degree of fouling of panels.

Characterizations

The molecular structures of the copolymers were characterized by FTIR spectroscopy using an IFS-113 FTIR instrument. The thermal performances of the copolymers were performed on a STA 449 synchronal thermal analyzer (NETZSCH company) under nitrogen flow of 50 mL min^{-1} at a heating rate of $10^\circ\text{C min}^{-1}$ from 30 to 900°C . The hydrophobicity of the copolymer was investigated by contact angle using data physics instruments OCA 20. The surface characteristics of the copolymers were measured after freeze-dried for 12 h by scanning electron microscope (SEM) and 3D measuring laser microscope OLS4000.

RESULTS AND DISCUSSION

Characterizations

FTIR Spectra. The resins were freeze-dried overnight, and the dried resins were ground into powder and mixed with KBr power. The mixed samples were compressed into small slices and analyzed by the FTIR spectrophotometer. The characteristic FTIR absorption peaks of C-1, C-2, C-3, and C-4 were detected in Figure 4(a): $-\text{CONH}_2$ (N—H stretching) at 3448 cm^{-1} ,

$-\text{COOH}$ (C—O stretching) at 1640 cm^{-1} , and $-\text{COOC}-$ (C—O stretching) at 1168 cm^{-1} . The preliminary results indicated that the spectrum had peaks characteristic of the monomers (AM, MAA, and BA) used in the C-1 formulation. In addition to the characteristic absorption peaks of C-1, the detection of peaks including $-\text{CONH}-$ (N—H stretching) at 2965 cm^{-1} , $-\text{C}=\text{C}$ stretching at 1734 cm^{-1} , and Ph—OH (C—O stretching and O—H bending) at 1463 cm^{-1} indicate that the spectrum had peaks characteristic of the monomers (AM, MAA, BA, and HDDE) used in the C-2 formulation. Moreover, the characteristic peak of R—OH (C—O stretching and O—H bending) at 1383 cm^{-1} suggested that the spectrum had peaks characteristic of the monomers (AM, MAA, BA, and N-MA) used in the C-3 formulation. However, the peak of R— SO_3H (S—O stretching) at 1268 cm^{-1} indicated that the spectrum had peaks characteristic of the monomers (AM, MAA, BA, and AMPS) used in the C-4 formulation. The characteristic FTIR absorption peaks of CT-1, CT-2, CT-3, and CT-4 were shown in Figure 4(b). Increase of $-\text{R}-\text{N}$ (C—N stretching) at 1160 cm^{-1} , N—H stretching and bending at 2971 and 1452 cm^{-1} . And $-\text{COOH}$ (C—O stretching) at 1640 cm^{-1} has disappeared in comparison with those of C-1, C-2, C-3, and C-4, illustrating that TTMAP has been grafted onto the resins.

Thermal Performances

The thermal stabilities of synthesized resins were investigated by TGA, and the results were used to determine the actual content of each polymer in the resins.²⁷ Figure 4(c) shows the TGA curves of C-1, C-2, C-3, and C-4. The synthesized resins presented evidently similar decomposition curves and multi-step degradation, arising from similar constituents. The weight of loss around 1.84 wt % in the temperature range of $35\text{--}200^\circ\text{C}$ was ascribed to the loss of absorbed moisture and elimination of water molecules from the hydroxyl and carboxylic groups. The weight loss of $\sim 12.19 \text{ wt } \%$ in the temperature range of $200\text{--}320^\circ\text{C}$ was attributed to the decomposition of side chains.

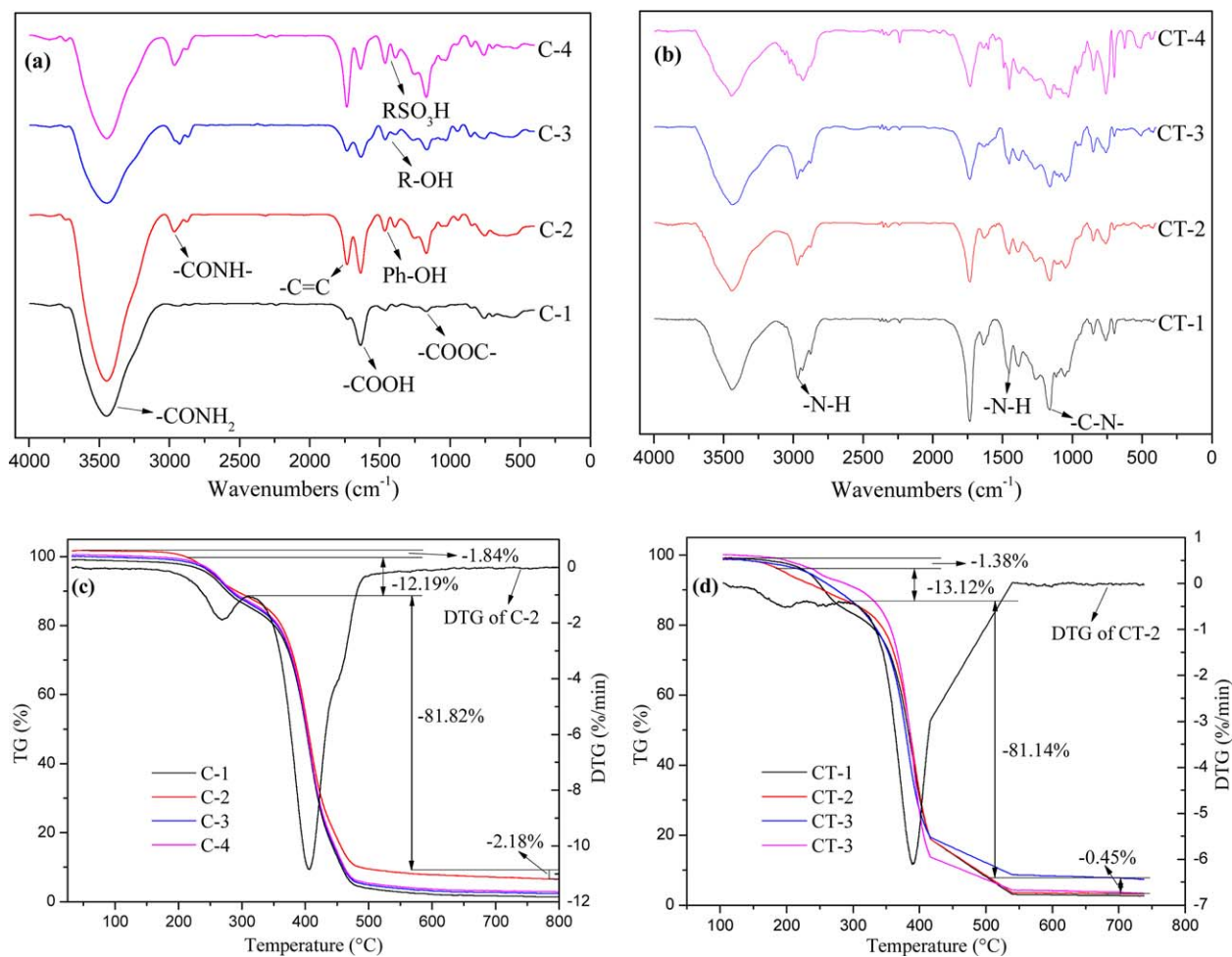


Figure 4. (a): FTIR spectra of C-1, C-2, C-3, and C-4; (b) TGA curves of C-1, C-2, C-3, and C-4. [Color figure can be viewed in the online issue, which is available at wileyonlinelibrary.com.]

The 81.82 wt % weight loss in the temperature range of 320–520 °C was increasingly significant because of the rupture of the main-chain backbone and the destruction of the crosslinked network.²⁸ The differential curve for C-2 indicated that the weight-loss temperature of C-2 at 245.7 °C was extended compared with those of C-1, C-3, and C-4, as well as much higher than those of other resins. The thermal stability of C-2 appeared to be greater than the other resins. This phenomenon was caused by the rigid structure and enhancement of hydrogen-bond interaction with the incorporation of HDDE. As shown in Figure 4(d) for the TGA curves of CT-1, CT-2, CT-3, and CT-4, the weight loss in the second stage of CT-2 (13.12 wt %) was larger than that of C-2 (12.19 wt %) and the differential curve for CT-2 indicated that the weight-loss temperature of CT-2 was at 205.1 °C, which were mainly attributed to the TTMAP grafted onto the resins. The change of weightlessness of the third stage (81.14 wt %) was basically consistent with that of C-2, indicating that there was no change in the main chain.

Surface Characteristics

SEM images for the section structures of the resins with or without crosslinker are shown in Figure 5, to demonstrate the dependence of resin morphology on the introduction of

TTMAP in the coatings. The crosslinked resins exhibit interpenetrated network structures compared with the uncrosslinked resins,²⁹ which can absorb hundreds to thousands times their own mass of water to preserve in their network space. They have compact structures in comparison with the uncrosslinked resins, especially those of CT-2 coating. Although it is difficult to reveal the molecular level structure from the SEM images, the interpenetrated structures of the hydrogels synthesized can still be demonstrated. The size and amount of pores evidently vary, and this phenomenon may be caused by the highly polar hydrogen bonding functionalities with each other or interact with surrounding nonpolar moieties, such as a benzene ring. Thus, the crosslinking porous structures in the resins increase the contact area with water, resulting in the decrease of contact angle and weakening their ability to self-peeling. Consequently, the confirmative hydrogel can achieve a higher expanded network and increased swelling ratio.

The functionality of a coating is highly dependent on layer thickness, coating uniformity, or coating porosity. Therefore, identifying the quality and microstructure of the coating is necessary to further understand the layer properties and process conditions.³⁰ Figure 6(a,b) display the confocal laser scanning

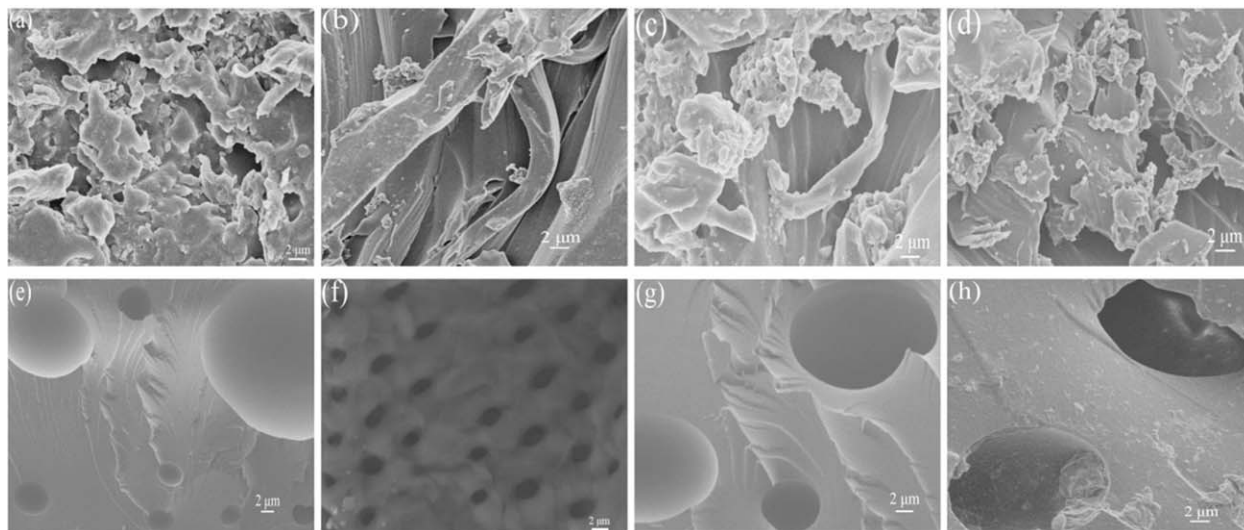


Figure 5. SEM photographs of the resultant resins: (a) C-1, (b) C-2, (c) C-3, (d) C-4, (e) CT-1, (f) CT-2, (g) CT-3, and (h) CT-4.

microscopy images of the coating surface after six cycles. The results indicate many variations in the abundance and distribution of microorganisms and the impurity in the biofouling layer during repeated immersion. Figure 6(a) shows high surface coverage by impurities and humus after six cycles, whereas CT-2 has the least topographical change as a result of biofouling because of the incorporation of HDDE with antibacterial and antifouling properties.²³ This conclusion can also be supported by the 3D image of CT-2 in Figure 6(b). However, the coating surfaces have become rough after six cycles in comparison with homogeneous, and no porosity of the coating before the experiment.

Contact Angle Analysis

When contacted with deionized water, the contact angle can be used to characterize the hydrophilicity or hydrophobicity of a coating. The hydrophilic variation of the coating can be identified by measuring the contact angle of the coating over different immersion times in degradation measurement. Figure 7(a,b) show that the contact angles are higher than 90° before immersion in seawater, suggesting a hydrophobic surface. The contact angle gradually becomes constant after six immersion cycles. Moreover, the contact angles of TMAP-modified resins are much larger than those of unmodified ones. This phenomenon is ascribed to the increased hydrophobic interactions within resins arising from

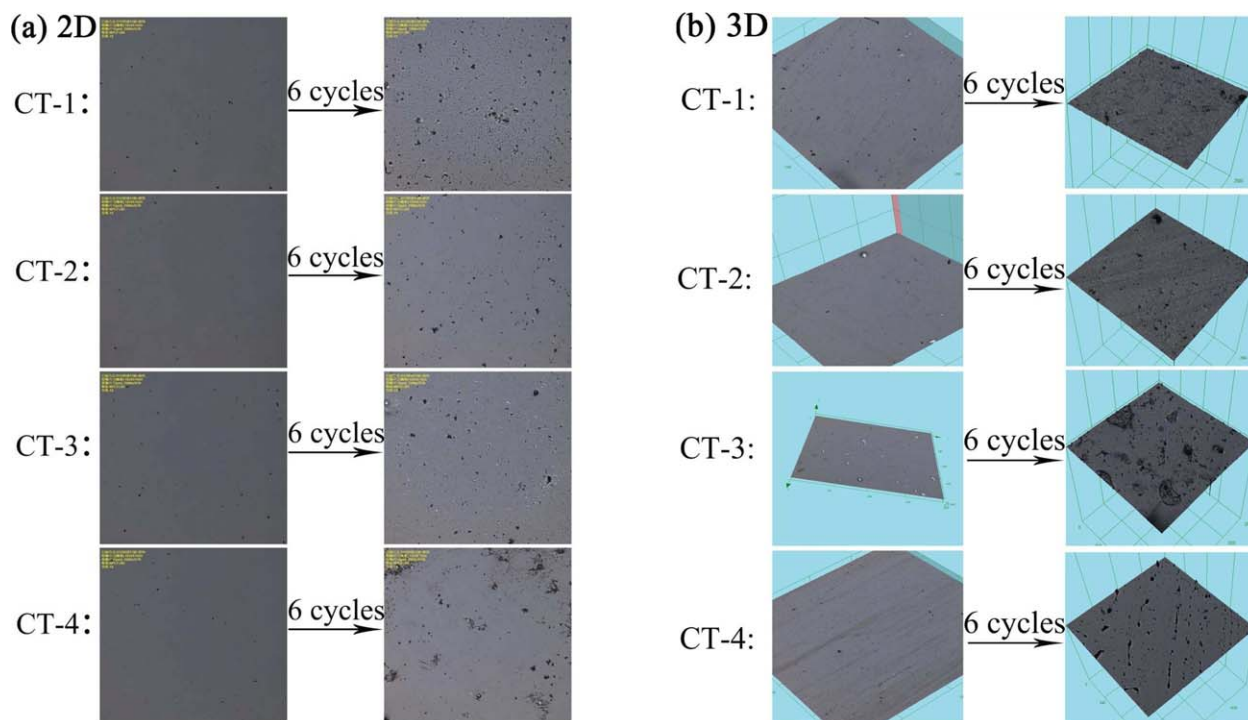


Figure 6. Schematic illustrations of surface morphology variations of 6 cycles: (a) 2D and (b) 3D modes. [Color figure can be viewed in the online issue, which is available at wileyonlinelibrary.com.]

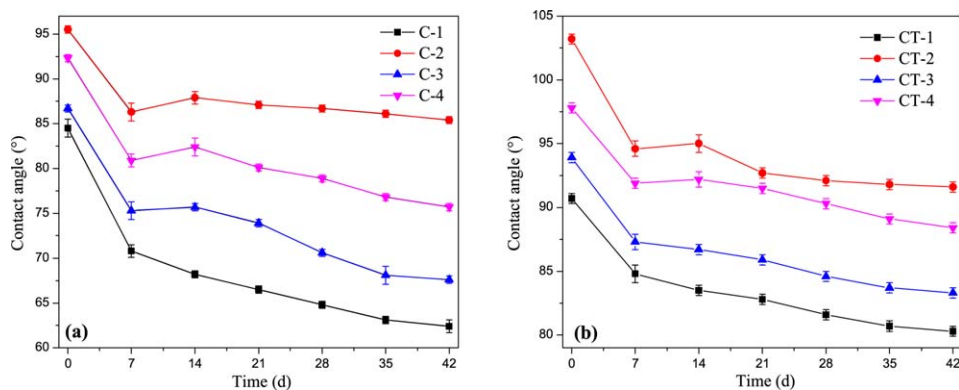


Figure 7. The contact angle deviations as a function of time. [Color figure can be viewed in the online issue, which is available at wileyonlinelibrary.com.]

the formation of crosslinked structures consuming the hydrophilic carboxylic acid groups and the higher contact angle and lower water content. The molecular chains of C-1, C-2, C-3, and C-4 have been sufficiently hydrolyzed to dissolve in seawater and leach out, or the presence of a biofilm of increasing thickness and complexity may have also contributed to a reduced water contact angle,³¹ which explains the difference among them in terms of contact angle. The crosslinked polymer chains can be hydrolyzed without leaching out compared with the uncrosslinked coating.

Adhesion and Stress

The grade tests of adhesion for CT-1, CT-2, CT-3, and CT-4 were performed in accordance with GB 1720-1979.³² The results show that the complete degrees of all coatings are one grade, indicating that CT-1, CT-2, CT-3, and CT-4 coatings show excellent adhesion property, especially CT-2 coating. CT-2 is an environment-friendly antifouling material with great development potential.

Figure 8(a) shows a representative plot of the stress of a series of uncrosslinked resins. The mechanical properties of these resins are much lower than those of crosslinked ones. Figure 8(b) shows that mechanical strength increases with increasing molar TTMAP/resin ratio. This phenomenon is mainly ascribed to the Michael addition reaction of the aziridine crosslinker and carboxyl groups with exact complete reaction to form a full 3D network when the TTMAP/resin mole ratio is 1:3.³³ The crosslinking reaction enhances abrasion resistance, water resistance, and adhesion force. The structures of uncrosslinked resins are looser and exhibiting larger pore spacing, thereby reducing the hydrogen-bond interactions and mechanical strength. Consequently, a suitable crosslinking density is favorable to improve the mechanical strength.

Dynamic Abrasion Property

Figure 9(a,b) illustrate an abrupt weight loss in the initial stage, which is presumably caused by a quick release of some low-molar-mass components, such as residual solvents and unreacted monomers.³⁴ The abrasion rates of the crosslinked coatings are much lower than those of the uncrosslinked ones. Figure 9(b) shows that a thin and soft layer of hydrogel formed when the samples were immersed in seawater because of the

crosslinking and elevated reacting temperature (90 °C) for coating synthesis. The under layer of the coatings, particularly CT-2, remains hydrophobic after the top hydrogel layer is removed. The individual regions display micropores, which are attributed

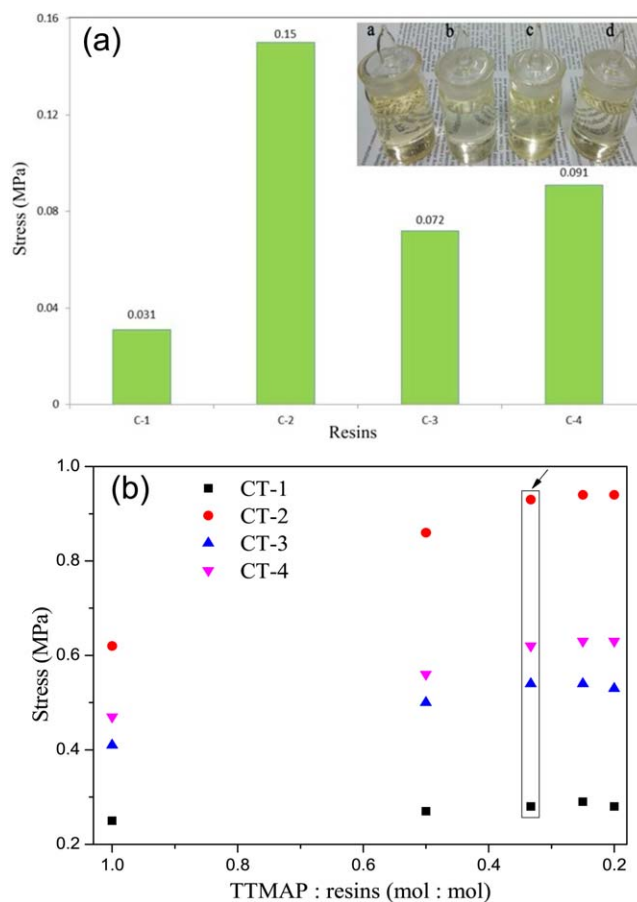


Figure 8. (a) Schematic illustrations of the stress of the uncrosslinked resins; **The inset** is typical appearance of the resins in the absence of crosslinker (i: C-1, ii: C-2, iii: C-3, iv: C-4). (b) The variation curves of the crosslinked resins with different crosslinker under the TTMAP/resins mole ratio at 1:1, 1:2, 1:3, 1:4, and 1:5. [Color figure can be viewed in the online issue, which is available at wileyonlinelibrary.com.]

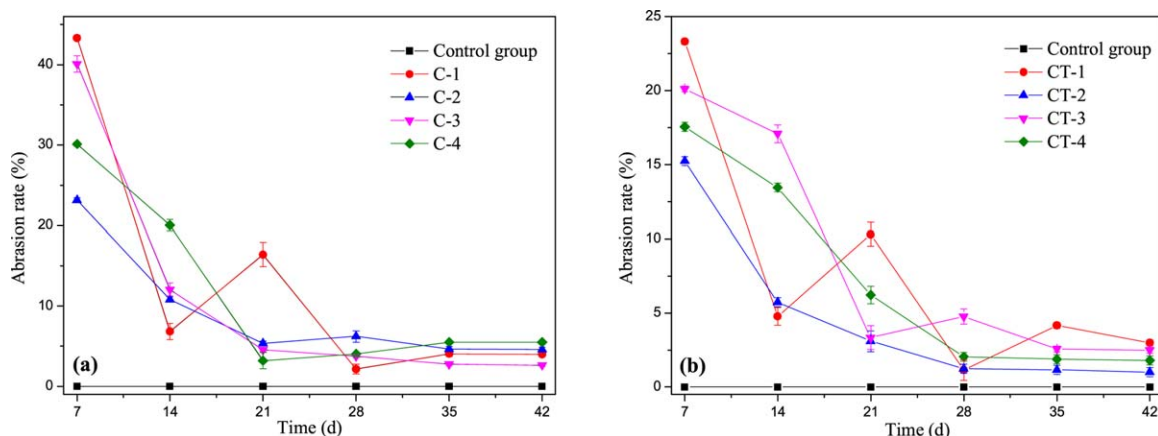


Figure 9. (a,b) The variation curves of abrasion rate over time. [Color figure can be viewed in the online issue, which is available at wileyonlinelibrary.com.]

to the bubbles entering the coating films. The surface of CT-1 coating showed tiny cracks after two cycles because the introduction of a large number of hard monomer AM and the cross-linked copolymer molecular chain reduces the flexibility of coating and increases brittleness. However, coupled with coatings removed from the seawater, sudden changes in humidity and temperature result in concentrated stress on the surfaces of the coatings, leading to the cracking of the coating surface. Many scratches form on the surface after stroking water and are easily washed away by the seawater because of the low cross-linked densities of CT-3 and CT-4 coatings. However, after four cycles of CT-2 coating, the surface of the coating is very smooth, with only a spot of scratches, indicating good abrasion resistance. This phenomenon is mainly ascribed to the incorporation of HDDE that can form high-density network-crosslinked structure under the action of TTMAP.

Static Degradation Property

Figure 10(a,b) schematically show the degradation rates between the crosslinked and uncrosslinked coatings when immersed in seawater. The weight loss of the coating is used to reflect the degradation property of the coating in the seawater. No obvious difference is observed in the variation trends of degradation rates. The degradation rates of crosslinked coatings in Figure

10(b) are significantly lower than those of the uncrosslinked coatings in Figure 10(a) because the surface of the crosslinked coatings swells to form a thin layer of soft and dynamic hydrogel and does not undergo self-peeling phenomenon. Fragments of crosslinked coatings start to be gradually washed away with the increased time, only after a large number of crosslinked bonds are hydrolyzed and broken, which leads to the lower layer of the new resin exposed, that is, displaying self-generating phenomenon. However, the copolymer chains in the uncrosslinked coatings swell to hydrolyze from the top to bottom layer and become soluble, thus showing greater weight loss. The difference in the coating surface can be seen intuitively in the SEM images (Figure 5). For coatings (e)–(h), the crosslinking of the coating is visible in the cross-section SEM images, but such hydrogel layer does not exist in coatings (a)–(d). In addition, the washing away of the uncrosslinked coating results in abundant holes and fragments on the surface of coatings (a)–(d). Self-polishing is gradually achieved as the coating is washed away.

Thus, the degradation rates of crosslinked coatings are slower than those of uncrosslinked coatings after 30 days. This phenomenon is ascribed to the fact that the initial hydrolysis only swells the top layer of the coating to form a hydrogel, not leading to much peeling into seawater because of the crosslinker.²²

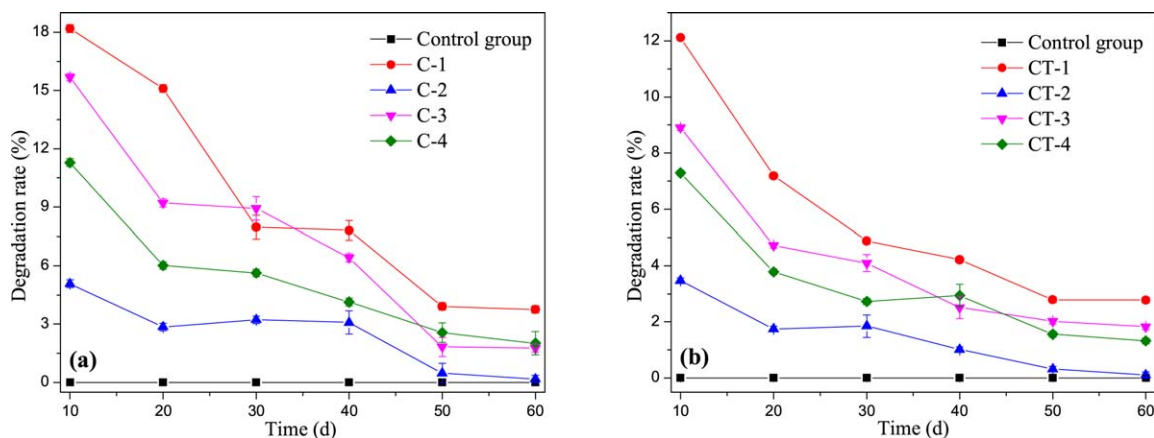


Figure 10. (a,b) The variation curves of degradation rate over time. [Color figure can be viewed in the online issue, which is available at wileyonlinelibrary.com.]

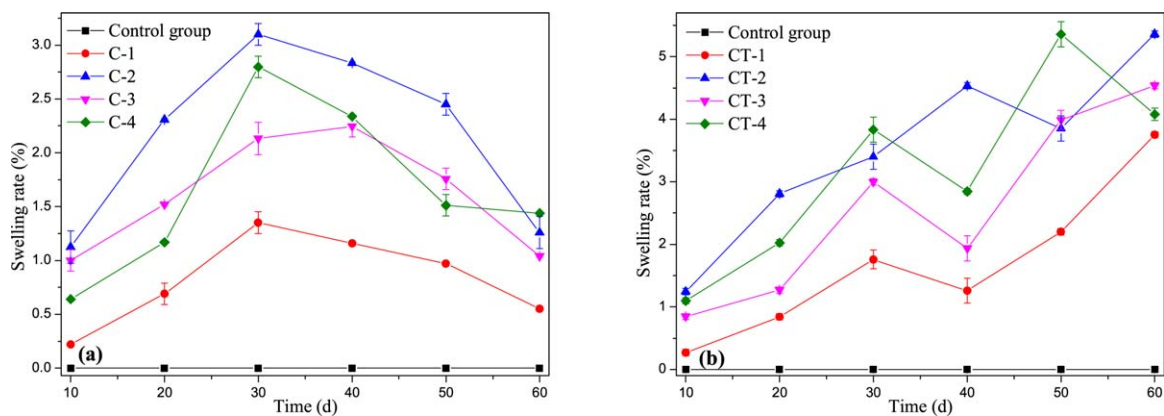

















Figure 11. (a,b) The variation curves of swelling rate over time. [Color figure can be viewed in the online issue, which is available at wileyonlinelibrary.com.]

Remarkably, the degradation rate of CT-2 coating is lower than those of the other coatings, indicating that CT-2 coating demonstrates better adhesion and mechanical strength. Moreover, HDDE is a di-substituted product, which can form a high degree of crosslinked network to increase the crosslinked points between the polymer chains. Therefore, the surface polymer layer is difficult to peel off into the seawater, leading to reduced weight loss. However, the stability of HDDE with phenyl structure and the enhancement of hydrogen bond interactions result in more compact crosslinked coating.

Swelling Property

Figure 11(a,b) show the swelling of the coatings in the seawater. The swelling rates gradually increase with immersion time for the crosslinked coatings. The hydrophilic groups of coating surface can adsorb considerable amount of water by hydrogen-bonding interactions. The water absorption decreases with further penetration of seawater because of the crosslink interaction between the polymer chains. This process results in the formation of a thin hydrogel layer at the coating surface, leading to increased thickness and water uptake. The swelling rate of CT-2

Table II. Results of Testing Panels in the Sea

Samples	0 days	30 days	60 days	90 days
Control group				
CT-1				
CT-2				
CT-3				
CT-4				

coating is higher than those of the other coatings, mainly because of the formation of dense crosslinked pores. The swelling rates of uncrosslinked coatings [Figure 11(a)] exhibit peaks during the swelling processes compared with the crosslinked coatings [Figure 11(b)]. Notably, competition processes exist between water absorption and leaching out of hydrolyzed copolymer chains. For the C-1, C-2, C-3, and C-4 coatings, the copolymer combines a small amount of water molecules to show slight swelling in early days. However, they cannot form a stable hydrogel layer because they are not crosslinked. In addition to the increase in immersion time, the increasing distance between the polymer chains leads to decreased interchain interaction. The polymer chains become loose and dissolve into the seawater, indicating that the weights of the coatings drop significantly, especially that of the C-1 coating.

Antifouling Property

Previous results show that the properties of crosslinked coatings are significantly enhanced compared with those of uncrosslinked coatings. Therefore, the crosslinked coatings (CT-1, CT-2, CT-3, and CT-4) have been used to perform the panel test in seawater, and the corresponding data are summarized in Table II. Table II shows that the control group is covered with various biofilms and substantial green marine algae, such as *Enteromorpha prolifera* and barnacles. No marine organisms are attached to the other panels within 30 days except for trace amounts of microbial mucosa and mud. This result suggests that CT-1, CT-2, CT-3, and CT-4 as antifouling materials can improve the antifouling properties of coatings. Hydrophilic nonfouling surfaces prevent the organic adsorption and biofouling by generating a soft and dynamic hydrogel layer.^{35–38} A connection between biofouling and retention/release bind water molecules from the surface.^{39,40} Other panels present a large number of microbial and algae attachment after 60 days. By contrast, the control group shows microorganism mucosa and barnacles instead of *E. prolifera*, indicating that the control group rarely demonstrates antifouling property. Afterward, biofilms and sludge in coatings CT-1, CT-3, and CT-4 are washed off by seawater over a period of 90 days. The coatings are evidently contaminated by more biological mucosa and barnacles compared with the coatings at 60 days. The coating surface is damaged and seriously abraded, which indicates reduced antifouling property. This phenomenon is well correlated to the more hydrophilic surface with more water molecules bound on the surface, directly reflected by the low contact angle and high water adsorption after immersion in seawater. However, CT-2 coating evidently shows lesser biological mucosa and barnacles than other coatings, indicating superior antifouling property of CT-2 compared with other coatings.

Given the unique and complex character of the real marine environment, it facilitates the gradual accumulation and colonization of organics and living matters (such as bacteria, single-cell diatoms, and protozoa) on the surface of coatings, forming a thin biofilm. Uncrosslinked coatings just present the self-polishing property and perform less effectively as an antifouling surface. Accordingly, the chains leach out when the hydrolysis reaches a certain degree. By contrast, the crosslinked coating prevents the leaching of highly hydrolyzed chains so that the surface is more negatively charged with abundant

tightly bound water molecules, making the adsorption of organics more difficult. Furthermore, a new layer of hydrogel can continuously self-generate because of the self-peeling property, which can maintain the nonfouling character of the surface. This result correlates well with its better antibiofouling ability.

CONCLUSIONS

A series of polyacrylamide-based resins with crosslinked porous structure has been successfully synthesized to integrate self-peeling and self-generating properties in a single coating. Enhancement of the thermal stability of modified resins is advantageous to increase mechanical strength and adhesion. The preliminary results from dynamic abrasion, static degradation, and swelling tests confirm that crosslinked coatings are promising for antifouling applications because of their properties which are superior to those of uncrosslinked ones. Moreover, the formation and peeling-off of a thin hydrogel layer on the coating surface can effectively slow down the biofouling performances. The incorporation of HDDE can markedly enhance antibacterial and antifouling properties of the coating.

ACKNOWLEDGMENTS

The authors would like to acknowledge financial supports from Natural Science Foundation of China (50673085, 41576077), National High-Tech Research and Development Program of China (2010AA09Z203), and the Fundamental Research Funds for the Central Universities of China (201562026).

REFERENCES

1. Champ, M. A. *Sci. Total Environ.* **2000**, 258, 21.
2. Yebra, D. M.; Kiil, S.; Johansen, K. D. *Prog. Org. Coat.* **2004**, 50, 75.
3. Chambers, L. D.; Stokes, K. R.; Walsh, F. C.; Wood, R. J. K. *Surf. Coat. Technol.* **2006**, 201, 3642.
4. Dobretsov, S.; Dahms, H. U.; Qian, P. Y. *Biofouling* **2006**, 22, 43.
5. Becker, K.; Wahl, M. *Biofouling* **1991**, 4, 275.
6. Henrikson, A. A.; Pawlik, R. J. *J. Exp. Mar. Biol. Ecol.* **1995**, 194, 157.
7. Petronis, S.; Berntsson, K. M.; Gold, J.; Gatenholm, P. *J. Biomater. Sci. Polym. Ed.* **2000**, 11, 1051.
8. Katsikogianni, M.; Missirlis, Y. F. *Eur. Cells Mater.* **2004**, 8, 37.
9. Hasan, J.; Crawford, R. J.; Ivanova, E. P. *Trends Biotechnol.* **2013**, 31, 295.
10. Cheng, G.; Zhang, Z.; Chen, S. F.; Bryers, J. D.; Jiang, S. Y. *Biomaterials* **2007**, 28, 4192.
11. Hawkins, M. L.; Fay, F.; Renel, K.; Linossier, I.; Grunlan, M. A. *Biofouling* **2014**, 30, 247.
12. Wu, J.; Lin, W. F.; Wang, Z.; Chen, S. F.; Chang, Y. *Langmuir* **2012**, 28, 7436.
13. Meyer, R. L.; Arpanaei, A.; Pillai, S.; Bernbom, N.; Enghild, J. J.; Ng, Y. Y.; Gram, L.; Besenbacher, F.; Kingshott, P. *Colloids Surf. B* **2013**, 102, 504.

14. Ebran, N.; Julien, S.; Orange, N.; Auperin, B.; Molle, G. *Biochim. Biophys. Acta* **2000**, *1467*, 271.
15. Brady, R. F. Jr.; Singer, I. L. *Biofouling* **2000**, *15*, 73.
16. Krishnan, S.; Weinman, C. J.; Ober, C. K. *J. Mater. Chem.* **2008**, *18*, 3405.
17. Ekblad, T.; Bergstroem, G.; Ederth, T.; Conlan, S. L.; Mutton, R.; Clare, A. S.; Ekblad, T.; Bergström, G.; Ederth, T.; Conlan, S. L.; Mutton, R.; Clare, A. S.; Wang, S.; Liu, Y. L.; Zhao, Q.; D'Souza, F.; Donnelly, G. T.; Willemsen, P. R.; Pettitt, M. E.; Callow, M. E.; Callow, J. A.; Liedberg, B. *Biomacromolecules* **2008**, *9*, 2775.
18. Katsuyama, Y.; Kurokawa, T.; Kaneko, T.; Gong, J. P.; Osada, Y.; Yotsukura, N.; Katsuyama, Y.; Kurokawa, T.; Kaneko, T.; Gong, J. P.; Osada, Y.; Yotsukura, N.; Motomura, T. *Macromol. Biosci.* **2002**, *2*, 163.
19. Murosaki, T.; Noguchi, T.; Kakugo, A.; Putra, A.; Kurokawa, T.; Furukawa, H.; Murosaki, T.; Noguchi, T.; Kakugo, A.; Putra, A.; Kurokawa, T.; Furukawa, H.; Osada, Y.; Gong, J. P.; Nogata, Y.; Matsumura, K.; Yoshimura, E.; Fusetani, N. *Biofouling* **2009**, *25*, 313.
20. Tang, Q. W.; Sun, X. M.; Li, Q. H.; Wu, J. H.; Lin, J. M. *Colloid. Surf. A* **2009**, *346*, 91.
21. Tang, Q. W.; Sun, X. M.; Li, Q. H.; Wu, J. H.; Lin, J. M. *J. Colloid Interface Sci.* **2009**, *339*, 45.
22. Xie, L.; Hong, F.; He, C.; Ma, C.; Liu, J.; Zhang, G.; Wu, C. *Polymer* **2011**, *52*, 3738.
23. Yu, X. L.; Yu, L. M.; Jiang, X. H. *App. Chem.* **2014**, *31*, 594.
24. GB/T1727-1992, General Preparation of Paint Film, **1979**.
25. GB/T5210-2006, Paints and Varnishes-Pull-Off Test for Adhesion, **2006**.
26. GB/T5370-85, Antifouling Panels in Shallow Submergence, **1985**.
27. Ying, H.; He, G.; Zhang, L.; Lei, Q.; Guo, Y.; Fang, W. *J. Appl. Polym. Sci.* **2016**, *133*, DOI: 10.1002/app.42951.
28. Mandal, B.; Ray, S. K. *Mater. Sci. Eng. C* **2014**, *44*, 132.
29. Zhang, G. Q.; Zha, L. S.; Zhou, M. H.; Ma, J. H.; Liang, B. R. *J. Appl. Polym. Sci.* **2005**, 1927.
30. Bück, A.; Tsotsas, E.; Sommer, K. In *Size enlargement*; Elvers, B., Ullmann's Encyclopedia of Industrial Chemistry Wiley-VCH, **2014**; pp 1–47.
31. Wang, W. Chinese Academy of Sciences, **2003**.
32. GB 1720-1979, Determination of Adhesion of Paint Film, **1980**.
33. Jia, L. N. Ocean University of China, **2014**.
34. Yonehara, Y.; Yamashita, H.; Kawamura, C.; Itoh, K. *Prog. Org. Coat.* **2001**, *42*, 150.
35. Hower, J. C.; Bernards, M. T.; Chen, S. F.; Tsao, H. K.; Sheng, Y. J.; Jiang, S. Y. *J. Phys. Chem. B* **2009**, *113*, 197.
36. Zheng, J.; Li, L. Y.; Chen, S. F.; Jiang, S. Y. *Langmuir* **2004**, *20*, 8931.
37. Ostuni, E.; Chapman, R. G.; Holmlin, R. E.; Takayama, S.; Whitesides, G. M. *Langmuir* **2001**, *17*, 5605.
38. Jeon, S. I.; Lee, J. H.; Andrade, J. D.; De Gennes, P. G. *J. Colloid Interface Sci.* **1991**, *142*, 149.
39. Besseling, N. A. M. *Langmuir* **1997**, *13*, 2113.
40. Vanderah, D. J.; La, H. L.; Naff, J.; Silin, V.; Rubinson, K. A. *J. Am. Chem. Soc.* **2004**, *126*, 13639.